Chemical Engineering Journal 381 (2020) 122777

Contents lists available at ScienceDirect

Chemical Engineering Journal

journal homepage: www.elsevier.com/locate/cej

Synthesis of a novel dual layered double hydroxide hybrid nanomaterial and its application in epoxy nanocomposites

Zhida Zhang[a], Jianyu Qin[a], Wenchao Zhang[a], Ye-Tang Pan[a,*], De-Yi Wang[b], Rongjie Yang[a]

[a] National Engineering Technology Research Center of Flame Retardant Materials, School of Materials Science & Engineering, Beijing Institute of Technology, Beijing 100081, PR China

[b] IMDEA Materials Institute, C/Eric Kandel, 2, 28906 Getafe, Madrid, Spain

HIGHLIGHTS

- NiCo-LDH nanosheets were anchored onto MgAl-LDH employing MOFs as a precursor.
- The unique nanostructure offered uniform dispersion and strong interfacial interaction.
- The hybrid was incorporated into epoxy resin to improve its flame retardancy.
- The existence of the hybrid had little impact on the mechanical properties of epoxy resin.

GRAPHICAL ABSTRACT

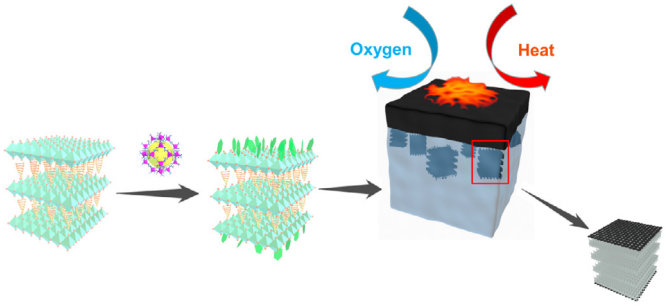

ARTICLE INFO

Keywords:
Epoxy resin
Metal organic frameworks
Layered double hydroxides
Nanocomposites

ABSTRACT

Ease of undesirable agglomeration and low efficiency are two problems that highly restrict the application of MgAl-layered double hydroxides (MgAl-LDH) as suitable flame retardants for epoxy resins. Herein, a new strategy that chose MOFs as the precursor to connect two different LDHs into a hybrid nanomaterial is reported. Nanosheets of NiCo-layered double hydroxides (NiCo-LDH) with multidimensional nanostructures were uniformly anchored on the surface of MgAl-LDH slabs. This led to a better dispersion and stronger interaction within the epoxy matrix, resulting in enhanced strength of the char layers, and also enabled synergistic flame retardant effect to the epoxy nanocomposite, when compared to the case of the unmodified epoxy. The sample passed V-0 rating in UL-94 test and its peak of heat release rate was reduced by 66.7% in cone calorimeter test with the addition of only 2.5 wt% of as-prepared flame retardant. Besides, due to the unique structure of the nanofiller, the mechanical properties of the nanocomposite were only slightly impacted. This is the first report on the synthesis of a dual LDH hybrid nanomaterial, which moreover, improved the flame retardancy of epoxy nanocomposite even when added in relatively low amounts.

1. Introduction

Epoxy resins (EP) are widely used in various areas, such as petrochemicals, electric and electronic appliances, construction, transportation and manufacturing. However, the flammability of epoxy resins seriously restricts their application [1,2]. The addition of flame retardants into epoxy resin can mitigate this situation [3,4]. Layered double hydroxides (LDHs) are regarded as one of the most cost-effective flame retardant additives for epoxy resins due to their relatively high efficiency and ease of accessibility [5,6]. LDHs can be potentially used

* Corresponding author.
E-mail address: 6120180038@bit.edu.cn (Y.-T. Pan).

https://doi.org/10.1016/j.cej.2019.122777
Received 3 June 2019; Received in revised form 14 August 2019; Accepted 8 September 2019
Available online 09 September 2019
1385-8947/

to impart flame retardant properties (by serving as heat sinks) to the hosting polymer by absorbing heat, releasing water, and forming a protective oxide layer which can prevent further degradation [7–9]. Nevertheless, its poor compatibility with the epoxy matrix, uneven dispersion caused by agglomeration in the composite, and the lack of strong char layers during combustion, have been found to be important drawbacks of LDHs, which cannot be overlooked [10–12].

Owing to their high surface energy and interlayer van der Waals interaction, hydrogen bonds or electrostatic attractions, 2D nanostructures of LDHs tend to re-stack and condense during processing into nanocomposites, which greatly decreases their performance in applications [13]. One way to achieve improved properties is to assemble these nano-building blocks into a three-dimensional (3D) architecture, which synergistically combines the advantages of both microstructures and nanostructures, paving the way to realizing the applications of these nanomaterials [14]. Compared to traditional methods, such as surface modification by surfactants or coupling agents, and intercalation of organic anions into interlayers, the fabrication of nanostructures on the surface of LDHs has been found to be advantageous and has hence emerged as a hot research topic.

Unlike the surface of graphene oxide, the laminates of LDHs have a certain amount of positive charges, which greatly obstructs loading of metal cations on them [15]. In order to solve this problem, different types of pretreatments have been carried out to anchor the metal cations on the positively charges surfaces of LDHs. Although laborious, these efforts were successful, since the flame-retardant efficiency improved significantly after the modification. Kalali et al. anchored Fe_3O_4 nanoparticles on MgAl-LDH using an indirect procedure *via* the calcination-regeneration of LDHs, and found that the maximum heat release rate and total smoke production of the EP composite with 8 wt% Fe_3O_4-loaded LDHs were decreased by 55% and 34%, respectively, when compared to those of pristine EP [16]. Li et al. self-assembled $Ni(OH)_2$ nanoparticles on LDH nanosheets by using citrate ions to create negative charges, and results of UL-94 test illustrated that the addition of only 3 wt% of flame retardant was sufficient for the EP matrix to attain V-0 label [17]. However, the pre-treatments before anchoring the metal cation on LDH laminates are generally tedious, which makes it difficult to scale-up production of the flame retardant. Moreover, this technique is restricted to the engineering 0D nanoparticles and cannot be applied to nanocasting multidimensional nanostructures on LDHs. In contrast to a simple 0D nanostructure, multidimensional nanostructures act more effectively as “spacers” to hinder interparticle agglomeration of LDHs also significantly improve the interfacial interaction with the polymer matrix [18]. Thus, a precise control of the location of the metal ions on the laminates of LDHs and the fabrication of multidimensional nanostructures therefrom, remain challenging problems.

In recent times, hybrid nanocomposites formed from multiple two-dimensional nanomaterials such as graphene-LDHs [19], MoS_2-LDHs [20] and graphene-MoS_2 [21] have attracted much attention from materials scientists. To the best of our knowledge, combining two LDHs to create a hybrid LDH-LDH nanomaterial has never been reported. In the area of flame-retardant materials research, with regard to the assembly of LDHs using graphene and MoS_2, combining two LDHs is recognized as the more efficient nano-hybrid flame retardant, especially in epoxy resin systems. When using a traditional co-precipitation method (Scheme 1a), irregular nucleation sites can lead to a random distribution of LDH nanosheets on the laminates, and the nanosheets will grow along the a and b axes following thermodynamic principles. In this work, we selected ZIF-67, a type of metal organic frameworks (MOFs) as a precursor with the aim to anchor the metal cation (Co^{2+}) on LDHs, to further transform it into NiCo-LDH nanosheets. It has been reported that the surface metal cations of LDHs are present in an unsaturated coordination state, and are therefore active sites for *in situ* nucleation [22,23]. The first step is the coordination of alkaline ligands with Mg^{2+} to generate an unstable chelate intermediate on the surface of LDHs, after which, the ligand is captured upon adding Co^{2+} to form ZIF-67. Accordingly, ZIF-67 transforms to 2D NiCo-LDH nanosheets to form a 3D nanostructure on the laminates of MgAl-LDH (Scheme 1b), and we named this novel synthesis technique as “3D fabrication method”. This strategy allows easy loading of metal ions, construction of a multidimensional nanostructure, and ensures homogeneous dispersion of nanosheets on the laminates of LDHs.

In this study, NiCo-LDH nanosheets were evenly loaded on MgAl-LDH taking advantages of the property of MOFs to inhibit agglomeration and to enhance interfacial interaction. Compatibility was improved by intercalating an anionic surfactant into the interlayers. The presence of Ni, Co elements endows the hybrid nanomaterial with a synergistic flame-retardant effect and helps in forming strong char layers in epoxy nanocomposite during combustion. Thanks to this novel LDH hybrid flame retardant, the flame retardancy of epoxy nanocomposite was greatly improved while only slightly impacting the mechanical properties.

2. Experimental

2.1. Materials

Magnesium nitrate hexahydrate (99.0%) and nickel (II) nitrate hexahydrate (98.0%) used in this study were procured from Infinity Scientific (Beijing) Co. Ltd. Cobalt (II) nitrate hexahydrate (≥98.0%) and sodium dodecyl benzene sulfonate (SDBS, 95.0%) were purchased from Shanghai Whistle Kashiwa Chemical Technology Co., Ltd. 2-methylimidazole (2-MIM, 98.0%) was provided by Beijing Huawei Ruike Chemical Co., Ltd. Absolute ethanol (AR), anhydrous methanol (AR), deionized water, sodium hydroxide (AR), and aluminum nitrate nonahydrate (AR) were obtained from Beijing Chemical Works. Diglycidyl ether of bisphenol A (E-44, epoxy equivalent = 0.44 mol/100 g) was purchased from Nantong Xingchen Synthetic Material Co., Ltd. 4,4-diaminodiphenylsulphone (DDS, 98.0%) was purchased from Wuhan Yuancheng Technology Development Co., Ltd.

2.2. Preparation of MgAl-LDH (MgAl)

SDBS (0.005 mol) was dissolved in 100 ml of deionized water in a three-necked flask, and the solution was magnetically stirred for 30 min at 60 °C. Magnesium nitrate hexahydrate (0.01 mol) and aluminum nitrate nonahydrate (0.005 mol) were dissolved in 100 ml of deionized water, and another solution of 0.1 mol of sodium hydroxide in 100 ml deionized water was prepared. The two solutions were then added into two constant pressure funnels and the solutions were added into the three-necked flask. The Mg and Al mixed solution was dropped into the SDBS solution in 30 min during which, the pH of the mixture was controlled at 10 ± 0.5 with sodium hydroxide solution. After magnetic stirring for 30 min, the mixture was aged at 80 °C for 20 h. The obtained precipitate was filtered, washed several times with absolute ethanol and deionized water, and dried at 50 °C for 6 h.

2.3. Preparation of MgAl-LDH@NiCo-LDH (MgAl@NiCo)

MgAl-LDH (0.7 g) was dissolved in 100 ml of deionized water, and the solution was sonicated and stirred for 20 min. Next, 2-MIM (0.02 mol) dissolved in 50 ml methanol, was added rapidly into the above solution followed by stirring for 30 min, following which, cobalt nitrate hexahydrate (0.005 mol) dissolved in 50 ml of methanol, was added. The mixed solution was stirred for 5 min followed by aging for 24 h. The purple solid was collected by centrifugation, washed several times with methanol and dried at room temperature; the sample so obtained was named MgAl@ZIF-67.

A known weight of MgAl@ZIF-67 (0.75 g) was dissolved in 80 ml of ethanol and sonicated for 15 min to which, 30 ml ethanol solution containing 0.002 mol nickel nitrate was added and stirred for 2 h. The green solid obtained was collected by centrifugation, washed three

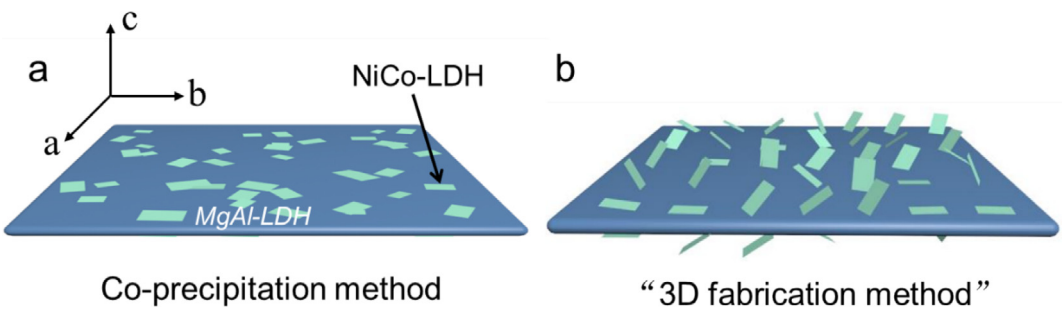

Scheme 1. Comparison of the two methods of preparation of LDHs hybrid nanomaterial.

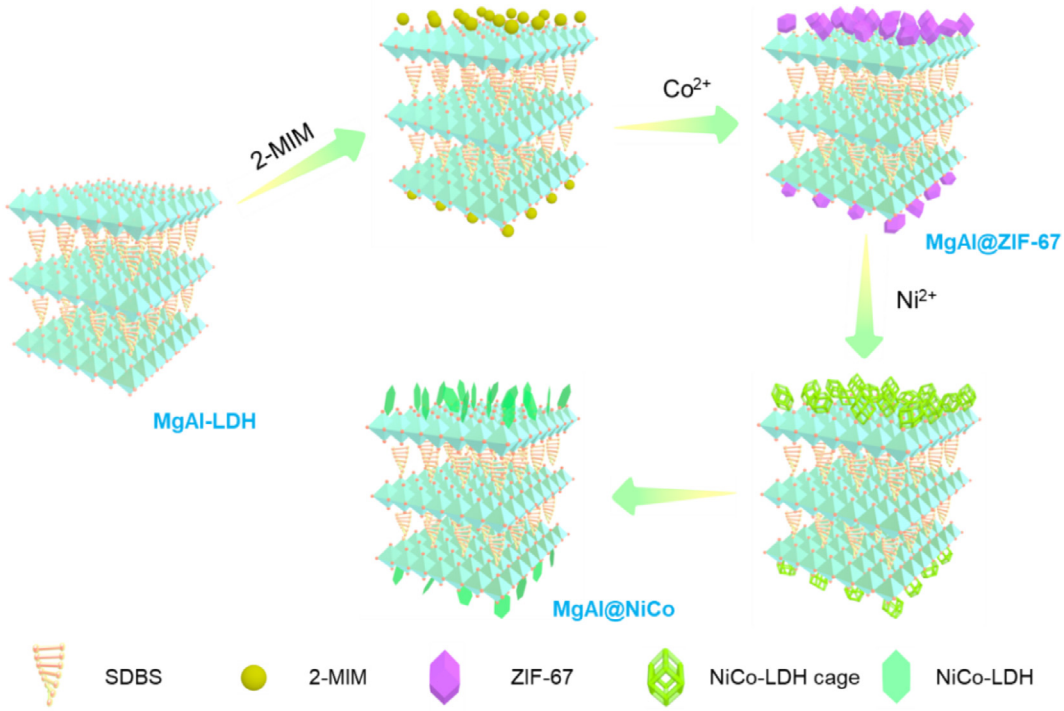

Scheme 2. Schematic of the preparation of MgAl@NiCo.

times with absolute ethanol and dried at 50 °C for 6 h. The sample so obtained was named MgAl@NiCo. The preparation process is illustrated in Scheme 2. NiCo-LDH without the addition of MgAl-LDH was also prepared.

2.4. Preparation of epoxy nanocomposites

Different mass fractions of MgAl@NiCo (2, 2.5 and 3 wt%) and MgAl (2.5 and 3 wt%) were first dispersed in epoxy resin under stirring at 140 °C for 2 h. The hardener DDS (ratio of DDS/epoxy was 30:100) was then added to the above solution. The mixture was stirred at 140 °C for 30 min to form a homogeneous liquid, which was heated in a vacuum oven at 120 °C for 20 min to remove bubbles and immediately poured into pre-heated molds of certain sizes. In the final step, the epoxy mixtures were cured at 180 °C for 4 h to form epoxy nanocomposites. The prepared samples were denoted as EP/2.5 (3)% MgAl and EP/2.5 (2, 3)% MgAl@NiCo.

2.5. Characterization

X-ray diffraction (XRD) patterns of the samples were obtained using Cu-K_α radiation (k = 1.54178 Å) on a MiniFlex 600 X-ray diffractometer operating at 40 kV and 15 mA (2θ range from 2° to 10° with a step size of 0.02°. Thermogravimetric analysis (TGA) was performed with a Net-zsch 209 F1 thermal analyzer; measurements were carried out in nitrogen atmosphere from 40 °C to 850 °C with a heating rate of 20 °C/min. A 5 mg sample was used for each measurement, and the gas flow rate was 50 ml/min. X-ray photoelectron spectroscopy (XPS) data were obtained using Perkin-Elmer PHI 5300 ESCA system at 250 W (12.5 kV at 20 mA) under vacuum ($< 10^{-6}$ Pa (10^{-8} Torr)). The sample was neutralized using both ion and electron guns. Scanning electron microscopy (SEM) images were taken with a Hitachi S-4800 (Hitachi Ltd., Japan) scanning electron microscope; samples were coated with a conductive gold layer and observed with a voltage of 15 kV. Transmission electron microscopy (TEM) images were obtained using a transmission electron microscope (HT7700, Hitachi, Ltd.) using a 120 kV electron source. Specimens were prepared by placing a drop of the sample in ethanol on a carbon-coated copper grid, and the grid was dried in air. LOI values were obtained using FTAII 1600 LOI instrument (Rheometric Scientific Ltd, England) according to ASTM D2863-97; the sheet dimensions were 125 × 6.5 × 3.2 mm^3. Vertical burning tests were performed using the UL-94 standard on samples of dimensions 125 × 13 × 3.2 mm^3. In this test, the burning grade of a material was classified as V-0, V-1, V-2 or no rating, depending on its behavior (dripping and burning time). Cone calorimeter measurements were performed according to the ISO 5660 protocol at an incident radiant flux of 50 kW/m^2. The equipment used was Fire Testing Technology (FTT) apparatus with a standard cone-shaped radiator. The specimen

($100 \times 100 \times 3\,mm^3$) was measured horizontally without any grids. Typical results from the cone calorimeter tests were reproducible to within ± 10%, and the reported data are averages from two measurements. Thermo-gravimetric analysis (Mettler-Toledo TGA/DSC-1) was coupled with Fourier-transform infrared spectroscopy (Bruker Tensor 27), and the measurements were carried out under nitrogen atmosphere from 50 °C to 800 °C at the heating rate of 20 °C/min^{-1}. The sample weight was 10 mg for each measurement. Raman spectra were recorded at ambient temperature on a Renishaw inVia confocal microscopy Raman system under excitation from with 632.8 nm-wavelength laser. Dynamic mechanical analysis (DMA) was carried out with a Rheometric Scientific DMTA V dynamic mechanical analyzer in shear mode. The dimensions of the specimens were $6.5 \times 6.5 \times 3.2\,mm^3$ and the measuring frequency was 1 Hz. Mechanical properties were measured using an electronic tensile testing machine (DXLL-5000, Shanghai D & G Measure Instrument Co. Ltd.) at the rate of 2 mm/min.

3. Results and discussion

3.1. Structural characterization of LDHs hybrid nanomaterial

The phase and composition of MgAl@NiCo were studied by XRD technique. The magnified pattern shown in Fig. 1a indicates reflections from the lattice planes, (0 0 3), (0 0 6) and (0 0 9) typical of LDHs. Notably, the interplanar distance of MgAl-LDH is larger than that of NiCo-LDH, as revealed by (0 0 3) at a lower 2θ value due to intercalation by the anionic surfactant. In the original and enlarged XRD patterns of MgAl@NiCo, (0 0 3) (0 0 6) from MgAl, (0 0 6) from NiCo could be clearly resolved, while peaks due to (0 0 9) from MgAl and (0 0 3) from NiCo overlapped. XRD patterns of the intermediate product MgAl@ZIF-67 was also recorded and compared with those of ZIF-67. Results showed that the characteristic peaks belonging to MgAl-LDH could be found in MgAl@ZIF-67. The above evidences prove that the two LDHs were successfully combined to form the hybrid nanomaterial. To study the preparation process of MgAl@NiCo, TEM images of ZIF-67, MgAl@ZIF-67 and the sample collected during the etching process after 1 h (MgAl@ZIF-67/NiCo) were taken and are shown in Fig. 1c–e, respectively. ZIF-67 particles are polyhedral with average size of ca. 500 nm. Following their immobilization on MgAl-LDH, ZIF-67 polyhedrons retained their shapes and are found uniformly anchored on MgAl-LDH platelets. Subsequently, these 3D polyhedrons were etched, collapsed and transformed into NiCo-LDH nanosheets.

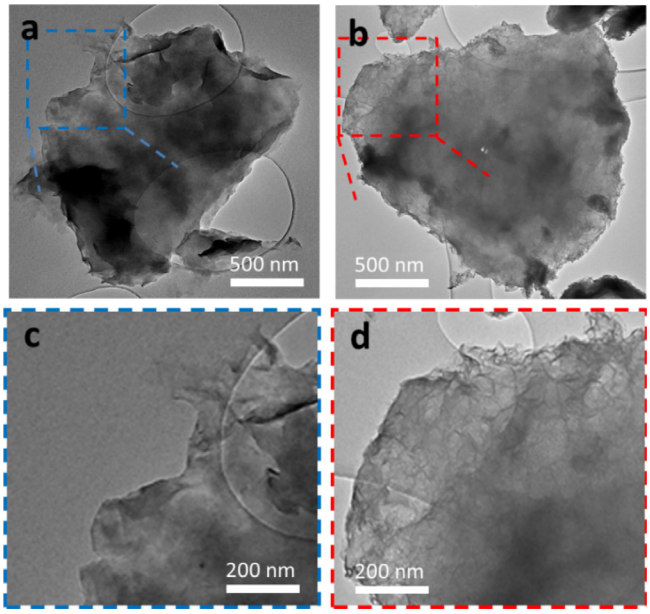

Fig. 2. TEM and magnified TEM images of (a and c) MgAl-LDH and (b and d) MgAl@NiCo.

To further confirm the structure of MgAl@NiCo, TEM images of MgAl-LDH and MgAl@NiCo were obtained (Fig. 2). Both samples display a lamellar 2D structure, but significant differences are seen on the

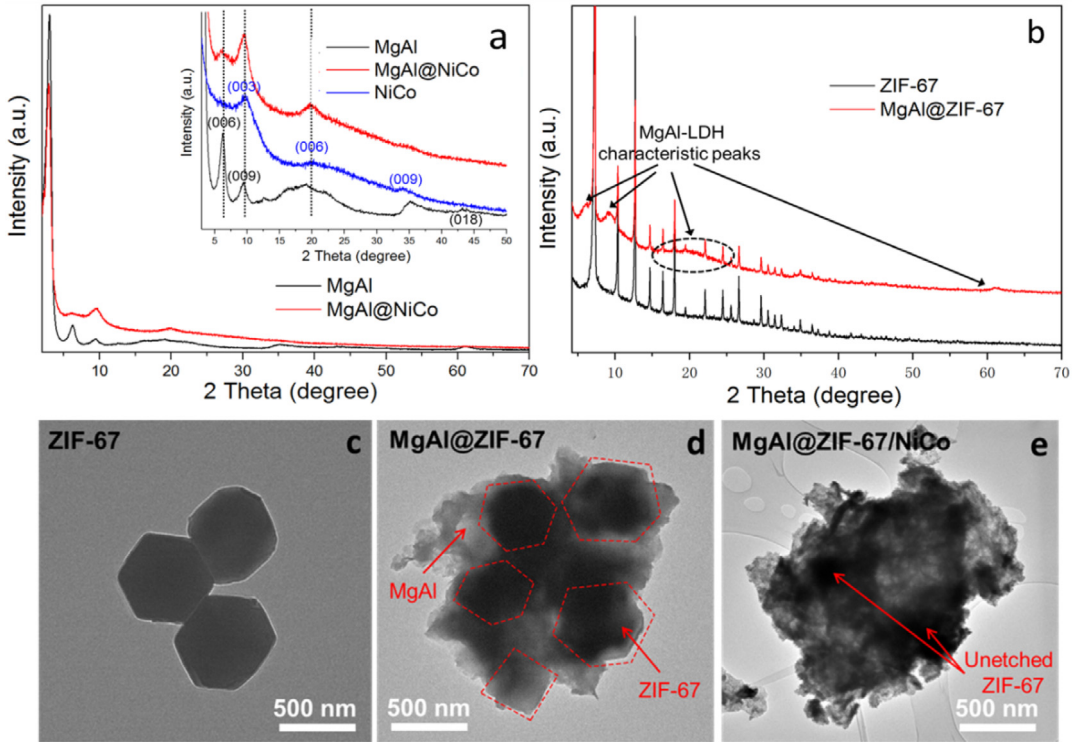

Fig. 1. XRD patterns of (a) MgAl. MgAl@NiCo and NiCo, (b) ZIF-67 and MgAl@ZIF-67; TEM images of (c) ZIF-67, (d) MgAl@ZIF-67 and (e) sample collected during the etching process after 1 h.

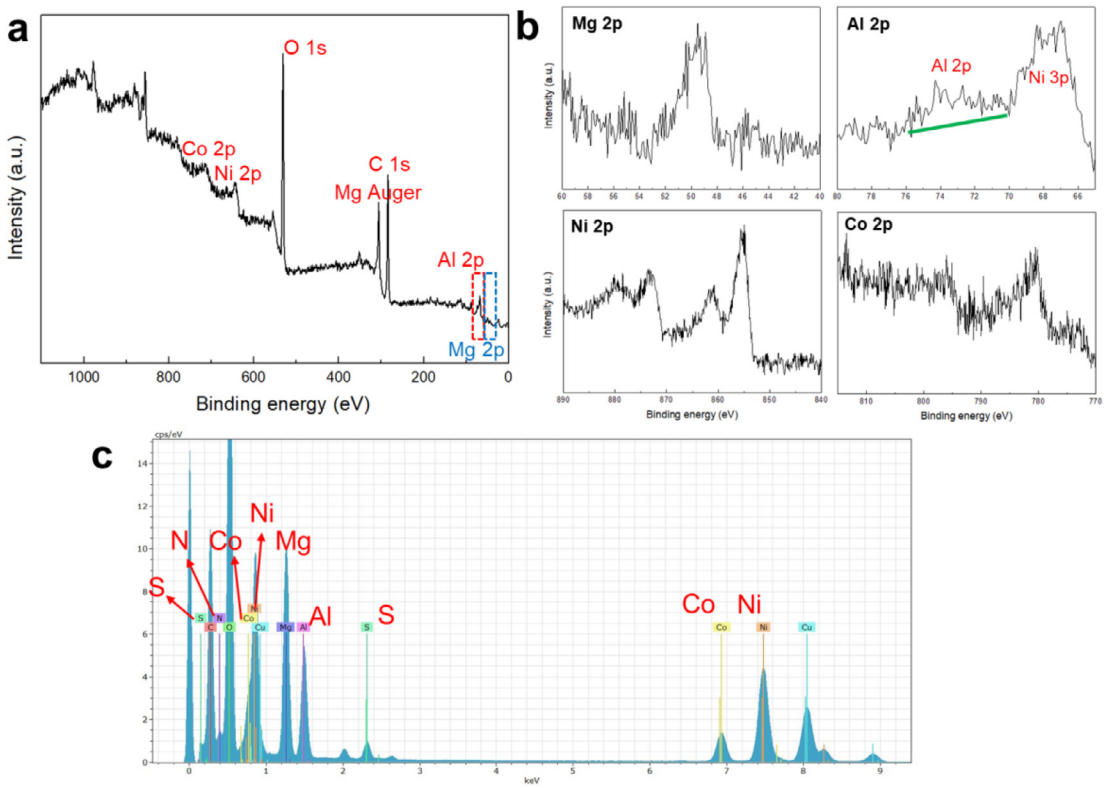

Fig. 3. (a) XP survey spectra, (b) Mg 2p, Al 2p, Ni 2p and Co 2p spectra of MgAl@NiCo and (c) TEM-EDX spectra of MgAl@NiCo.

surfaces of the laminates in the magnified images: The surface of MgAl-LDH with the lateral size of ca. 2 μm was smooth while that of MgAl@NiCo was fairly rough. The nanoplatelets clearly detected on the surface of MgAl@NiCo were found to be NiCo-LDH. NiCo-LDH nanosheets are found uniformly distributed on the laminates of MgAl-LDH to form a 3D nanostructure. This unique design played a vital role in preventing the agglomeration of LDHs, leading to their better dispersion in the nanocomposite and thereby enhanced their interfacial interaction with the epoxy matrix.

The elemental composition of MgAl@NiCo was identified from XPS spectra and TEM-EDX spectra. From XP survey spectra shown in Fig. 3a and b, the presence of Mg, Al, Ni and Co elements were confirmed. EDX spectra were also recorded to further confirm the elemental composition of MgAl@NiCo. As shown in Fig. 3b, the spectra clearly reveal the co-existence of Mg, Al, Ni and Co.

In order to study the nanostructure of MgAl@NiCo in detail, a typical particle was chosen for TEM investigations. The lattice fringes shown in high resolution TEM (HRTEM, Fig. 4b) image are correspond to the (0 1 8) plane of MgAl-LDH with d = 0.198 nm and (0 1 2) from NiCo-LDH with d = 0.258 nm; these values are in accordance with XRD data. The diffraction ring depicted in the selected area electron diffraction (SAED) pattern (Fig. 4c) also confirms this result. High angle annular dark field (HAADF) images of the elemental mapping of MgAl@NiCo demonstrates the uniform dispersion of Ni and Co, implying that our preparation procedure led to the uniform coverage of NiCo-LDH nanosheets on the whole surface of MgAl-LDH. The NiCo-LDH nanosheets loading was determined from TGA curves. As shown in Fig. 8a, all the samples exhibit the classic two-stage decomposition process of LDHs; at low temperature, the interlayer water is desorbed, and at high temperature interlayer anions are lost and the metal hydroxide layer is dehydroxylated. On the basis of the obtained residues, the theoretical loading of NiCo-LDH was calculated to be around 25.7 wt%.

3.2. Dispersion of LDH hybrid material in epoxy nanocomposites

The state of dispersion nanoparticles in a polymer matrix is one of the most important factors that determines the major chemical and physical properties of nanocomposites. Thus, the XRD patterns of epoxy and nanocomposites offer preliminary information on the nature of MgAl and MgAl@NiCo in the system. All the patterns showed the same amorphous phase of the epoxy resin, whereas the different peaks were observed at 2θ values < 10° for MgAl-contained sample and at 62° for both MgAl- and MgAl@NiCo-containing samples. The two peaks of EP containing 2.5 wt% MgAl at ca. 6° and 9° are ascribed to the (0 0 6) and (0 0 9) planes of MgAl-LDH, illustrating the presence of bulk agglomerates with several layers of LDHs in the epoxy matrix. In contrast, no peaks can be seen at 2θ < 10° for EP/2.5% MgAl@NiCo, probably because the nanofiller was well exfoliated and uniformly dispersed in the epoxy [24]. Notably, the peak at ca. 62° was present in both nanocomposites, but the one in MgAl@NiCo-containing sample had a lower intensity (Fig. 5).

To further study the state of dispersion of the additives, TEM images were obtained for the nanocomposites. In Fig. 6a and b, it is seen that MgAl-LDH in the polymer has a lamellar morphology, but the nanosheets aggregate into big particles with lateral sizes > 1 μm. Shown in Fig. 6c and d, particles MgAl@NiCo have much smaller sizes and are well dispersed. These results are in good agreement with XRD data. Thus, using the nanocasting method introduced in this work, an even dispersion of modified LDHs on the nanoscale achieved in the epoxy matrix. The NiCo-LDH platelets with 3D nanostructures increased the surface roughness of MgAl-LDH slabs, impeding their tendency to agglomerate and thereby enhanced the interfacial interaction with the matrix, which was found have a beneficial effect on various properties.

3.3. Fire safety of epoxy nanocomposites

The fire behaviors of epoxy nanocomposites were first surveyed using LOI and UL-94 tests. From the results shown in Table 1, we

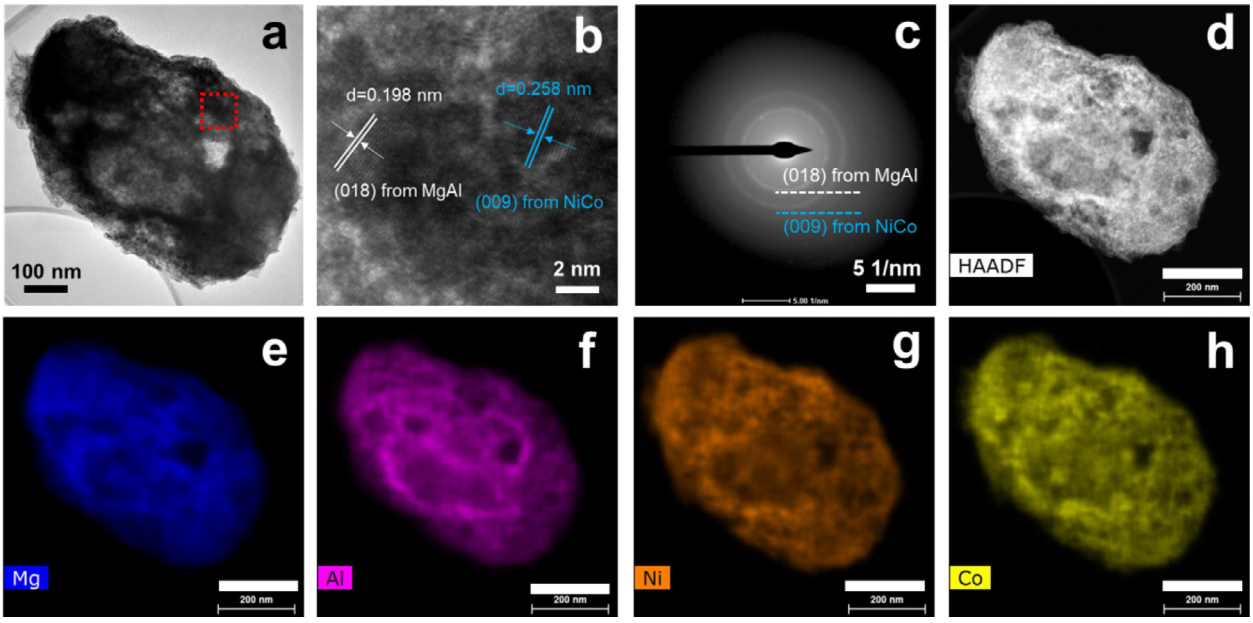

Fig. 4. (a) TEM image, (b) HRTEM image, (c) SAED pattern, (d–h) HAADF and elemental mapping (scale bar: 200 nm) of MgAl@NiCo.

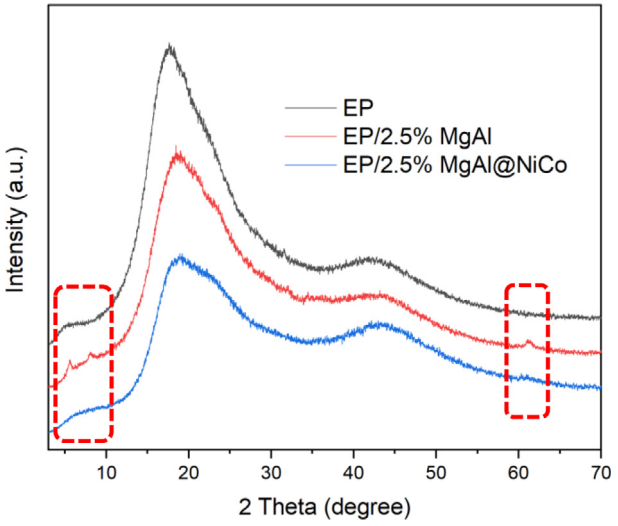

Fig. 5. XRD patterns of EP and its nanocomposites.

conclude that the addition of MgAl and MgAl@NiCo increases the LOI values of EP. Interestingly, when the added amounts of MgAl@NiCo were decreased from 3 wt% to 2.5 wt%, the LOI values of the nanocomposites increased to some extent, indicating that a number of agglomerated grains were exfoliated, which improved flame retardancy. The LOI value of EP/2.5% NiCo was lower than that of EP/2.5% MgAl, while the LOI value of EP/2.5% MgAl@ZIF-67 was higher than that of EP/2.5% MgAl, but lower than that of EP/2.5% MgAl@NiCo. In contrast to NiCo nanosheets, ZIF-67 on MgAl possessed a large particle size and also has an organic ligand, both of which might be detrimental to the flame retardancy of MgAl@ZIF-67. Addition of 3 wt% MgAl did not enable EP to achieve any rating in the UL-94 test, while EP containing 3 wt% MgAl@NiCo achieved V-0 rating without dripping. It is worth noting that the nanocomposite with a reduced MgAl@NiCo dosage of 2.5 wt% still maintained this performance. Even 2 wt% of as-prepared additive was able to endow EP with V-1 rating. Since 2.5 wt% of flame retardant-containing samples exhibited satisfactory results in LOI and UL-94 tests, cone calorimeter test was further carried out on these samples to further investigate their fire performance.

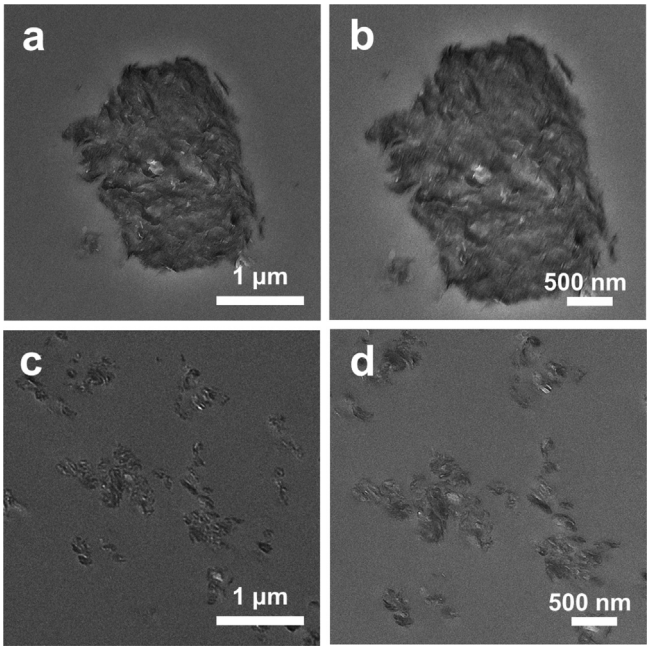

Fig. 6. TEM and magnified TEM images of (a and b) EP/2.5% MgAl and (c and d) EP/2.5% MgAl@NiCo.

Table 1
LOI and UL-94 test results of EP and its nanocomposites.

Sample	LOI (%)	UL-94	
		Rating	Dripping
EP	23.5	No rating	Yes
EP/3% MgAl	25.7	No rating	No
EP/3% MgAl@NiCo	25.3	V-0	No
EP/2.5% MgAl	25.4	No rating	No
EP/2.5% NiCo	25.2	No rating	No
EP/2.5% MgAl@ZIF-67	25.5	No rating	No
EP/2.5% MgAl@NiCo	26.0	V-0	No
EP/2% MgAl@NiCo	25.7	V-1	No

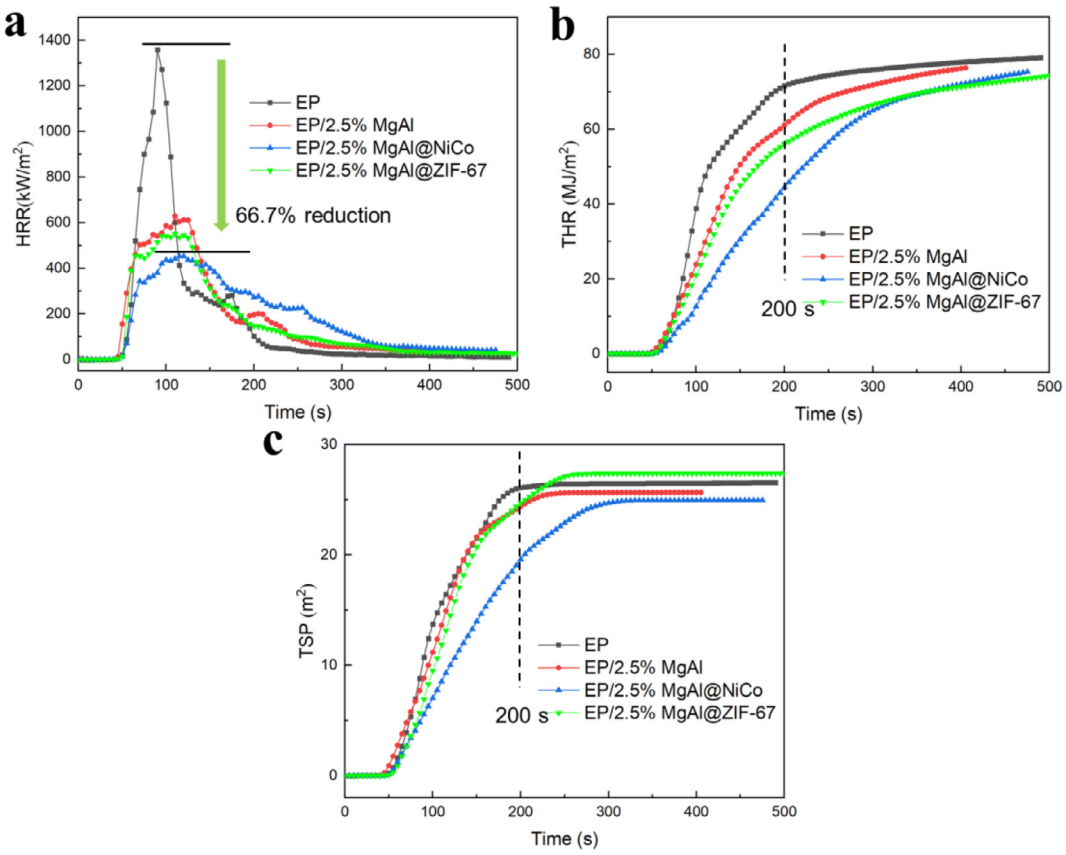

Fig. 7. (a) HRR, (b) THR and (c) TSP curves of EP nanocomposites.

The heat release rate (HRR), total heat release (THR) and total smoke production (TSP) curves of epoxy nanocomposites are shown in Fig. 7. The HRR curves (Fig. 7a) of both EP and EP/2.5% MgAl show two peaks; the lower intensity peak can be attributed to the breaking of the fragile char layer. The curve obtained for EP/2.5% MgAl@NiCo however, shows a different trend: In this case, once the char was formed, it continuously mitigated the release of heat, and consequently, the second peak is not clearly observed. The peak of heat release rate (pHRR) of EP decreased from 1361 to 628 kW/m^2 after adding 2.5 wt% MgAl, and further decreased to 455 kW/m^2 (66.7% reduction) with the addition of 2.5 wt% MgAl@NiCo, indicating that the fire hazard of epoxy nanocomposites can be reduced in a real flame scenario. In addition, the THR value at 200 s shown in Fig. 7b is reduced from 72.9 to 44.7 MJ/m^2 with the incorporation of MgAl@NiCo, and the corresponding value for the MgAl-incorporated sample is 61.4 MJ/m^2. Besides, EP/2.5% MgAl@NiCo also shows a lower TSP value at 200 s (19.8 m^2) as compared to those of the other two samples (Fig. 7c). EP/2.5% MgAl@ZIF-67 was also studied as a control sample and its pHRR value was higher than that of EP/2.5% MgAl@NiCo with a THR value at 200 s, but the results were better than those of EP/2.5% MgAl. Moreover, EP/2.5% MgAl@ZIF-67 released more smoke than EP/2.5% MgAl@NiCo at 200 s, similar to the value of EP/2.5% MgAl.

From the data listed in Table 2, it is seen that the amounts of char residue of EP/2.5% MgAl and EP/2.5% MgAl@NiCo increase from 4.9 to 9.8 and 10.9%, respectively, when compared to that of neat EP. In addition, the average mass loss rate (AMLR) that reflects the integral fire intensity and the fire growth index (FIGRA) that determines the fire spreading profile were, respectively, decreased by 37.9% and 73.6% with the addition of 2.5 wt% MgAl@NiCo into the epoxy, but were higher than the corresponding values observed for EP/2.5% MgAl. Thus, summarizing the results obtained from the fire tests, we conclude that MgAl@NiCo has a higher flame retardant efficiency than MgAl in epoxy resin at 2.5 wt% of the added amount.

3.4. Thermal stability of epoxy nanocomposites

The thermal stability of epoxy nanocomposites was monitored from TGA profiles traced under nitrogen atmosphere (Fig. 8b). All the samples showed a one-stage thermal decomposition process, mainly attributed to the degradation of the macromolecular chains [25]. For both the nanocomposites, the onset decomposition temperature ($T_{5\%}$, the temperature at 5% mass loss) was lower than that of neat EP due to the faster thermal degradation of LDHs and the catalytic effect of the metals. Despite the strong catalytic effect of the transition metals

Table 2
Cone calorimeter data of EP and its nanocomposites.

Sample	EP	EP/2.5% MgAl	EP/2.5% MgAl@ZIF-67	EP/2.5% MgAl@NiCo
pHRR (kW/m^2)	1361 ± 37	628 ± 26	555 ± 19	455 ± 29
THR (MJ/m^2) at 200 s	72.9 ± 2.7	61.4 ± 1.9	57.3 ± 1.7	44.7 ± 1.6
TSP (m^2) at 200 s	26.4 ± 0.8	24.5 ± 1.3	25.0 ± 1.2	19.8 ± 1.1
Char Residue (%)	4.9 ± 0.2	9.8 ± 0.3	10.0 ± 0.2	10.9 ± 0.3
AMLR (g/s)	0.103	0.073	0.071	0.064
FIGRA (kW m^{-2} s^{-1})	14.8	5.7	5.1	3.9

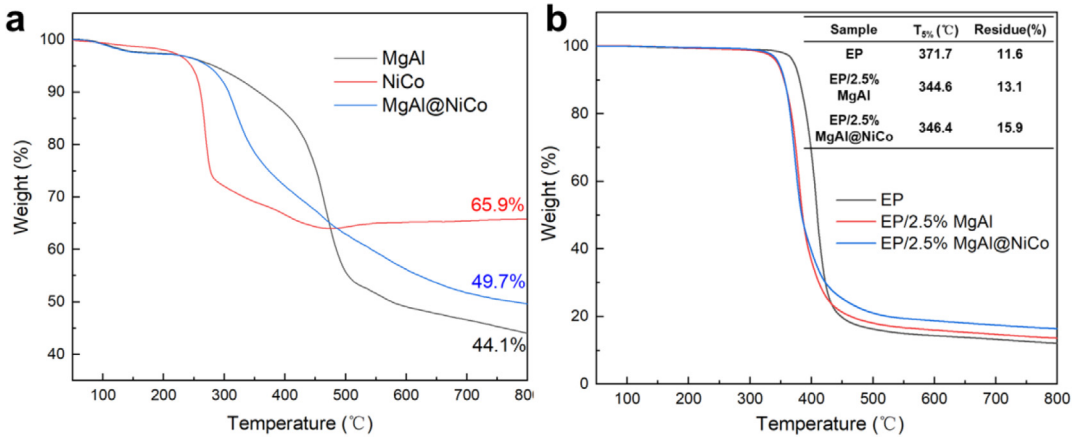

Fig. 8. (a) TGA profiles of sample powders, (b) TGA profiles of EP and its nanocomposites.

contained in MgAl@NiCo, the $T_{5\%}$ value of EP/2.5% MgAl@NiCo was a little higher than that of EP/2.5% MgAl probably owing to the better dispersion of MgAl@NiCo to function as a barrier inhibiting the movement of the epoxy molecular chain. The addition of 2.5 wt% MgAl@NiCo led to higher residue content for the nanocomposite than neat EP which is consistent with the result obtained from cone calorimeter test.

3.5. Condensed phase analysis

The residual chars of the neat epoxy and nanocomposites after cone calorimeter tests were collected and compared from different visual angles as shown in Fig. 9. It can be seen that neat EP shows a nearly total burnt out with a fragmentary structure, while the other two flame retarded samples have much more char yields in favor of serving as isolated layers. At first sight from the front view in Fig. 9e and f, the char residue of EP/2.5% MgAl@NiCo appears to be more compact and intumescent than that of EP/2.5% MgAl. The inset shows digital images of the prepared samples for strength test of the char and the resultant curves are depicted in the inset of Fig. 9f. The char strenghs of EP/2.5% MgAl@NiCo and EP/2.5% MgAl are as high as 14 N and 11 N; this result also implies that the former had more robust char layers. The

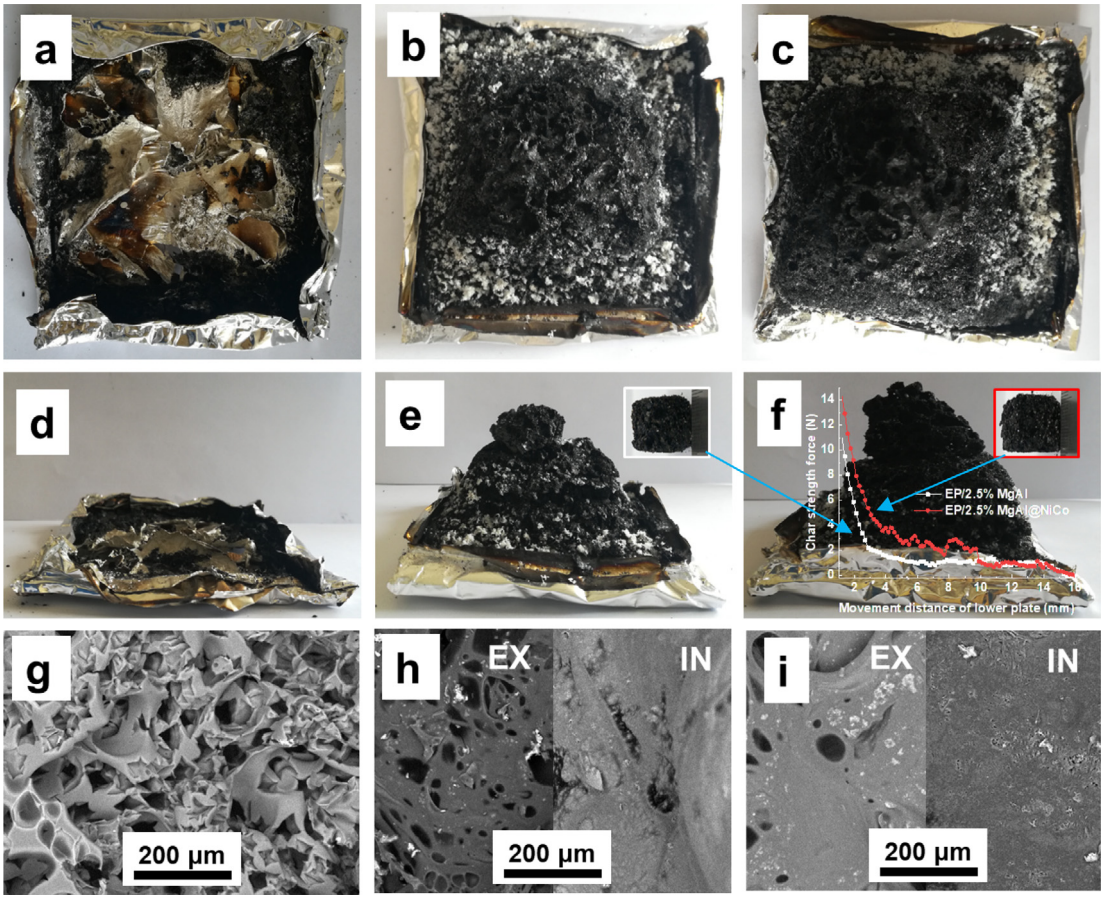

Fig. 9. (a) Top view and (d) front view of char from EP after the cone calorimeter test, (b) top view and (e) front view of the char from EP/2.5% MgAl, inset: Sample for strength test of char, (c) top view and (f) front view of char from EP/2.5% MgAl@NiCo and strength test result of char, inset: Sample for strength test of char, (g) SEM image of char from EP, (h and i) SEM images of exterior (EX) and interior (IN) char from EP/2.5% MgAl and EP/2.5% MgAl@NiCo, respectively.

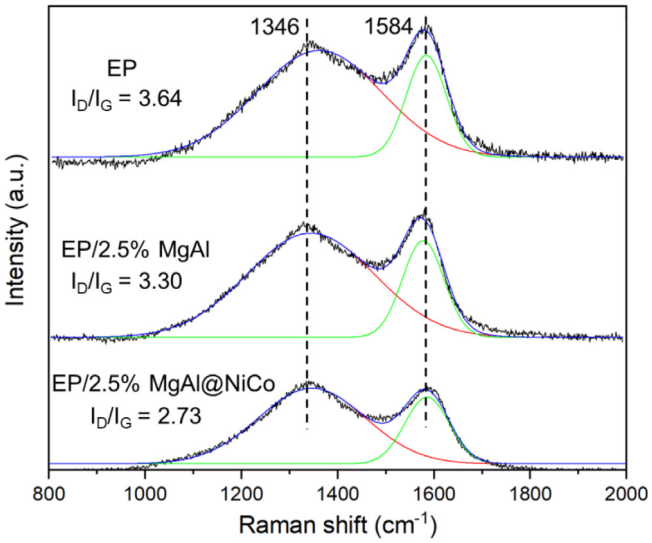

Fig. 10. Raman spectra of the char residues of EP and its nanocomposites.

microstructures of the char layers were further observed by SEM and the images are shown in Fig. 9g–i. The exterior and interior char of EP/2.5% MgAl@NiCo are more continuous and compact than those of EP/2.5% MgAl. In particular, large number of small pores were formed in the interior char of EP/2.5% MgAl@NiCo after burning, which is in accordance with its HRR curve indicating that heat was slowly released through these channels. The high quality char was conducive to slowing the exchange rate of heat and oxygen and to thereby improve the flame retardant performance of the nanocomposite [26,27].

The char residues were also characterized by Raman spectroscopy, which is a powerful characterization tool, especially for carbonaceous materials. As shown in Fig. 10, the Raman spectra of all the three samples show a D band at 1346 cm^{-1} and a G band at 1584 cm^{-1}. The D band is attributed to vibrations of the amorphous char, and the G band arises from the vibration of sp^2-hybridized carbon atoms. I_D/I_G is the ratio of the integral peak areas of the D and G bands. A lower value is proof of a higher graphitized carbon content. Among the three samples, the char sample of EP/2.5% MgAl@NiCo has the lowest I_D/I_G value. The transition metals (Ni and Co) in the flame retardant acted as catalysts to generate more graphitized carbon during combustion of the polymer. The presence of more graphitized carbons leads to enhanced thermal stability of the char structure. The char layer with a high thermal stability can act as a barrier to mass and heat transfer between the gas phase and the condensed phase.

The exterior and interior residual chars of EP containing 2.5 wt% MgAl and MgAl@NiCo were further investigated by XPS and the data are summarized in Table 3. The characteristic C1s bands at 284.6, 286.8 and 288.4 eV are ascribed to C—H and C—C in aliphatic and aromatic species, C—O (ether and/or hydroxyl group) and C═O, respectively [28]. To study the thermal oxidative resistance, C_{ox}/C_a (C_{ox}: oxidized carbons and C_a: aliphatic and aromatic carbons) values were calculated. The C_{ox}/C_a values of the exterior and interior residual char of EP/2.5% MgAl@NiCo were 0.63 and 0.49, respectively, which are much lower than those of EP/2.5% MgAl (1.41 and 0.91). The metal contents of metals in the exterior char were higher than those in the interior char, since the flame retardants migrated upward to the frontline of combustion. As a result, the accumulation of an inorganic layer made of by oxides on the surface of the char improved the thermal oxidative resistance of the protective char layer, which effectively served to inhibit oxygen permeation, heat and mass transmission, and the release of combustible gases from the matrix.

3.6. Vapor-phase analysis

TG-FTIR was employed to analyze the gaseous products formed during the thermal degradation process. As shown in Fig. 11, FTIR spectra were obtained during the thermal decomposition of EP and its nanocomposites at the maximum rate of evolution of gaseous products. Several small molecular gaseous produces were evolved during the decomposition from EP and its nanocomposite, clearly indicated by their were characteristic strong FTIR signals, such as —C—H groups for allyl alcohol, acetone and various hydrocarbons (3100–2800 cm^{-1}), CO_2 (2360 cm^{-1}), CO (2190 cm^{-1}) and aromatic compounds (1605, 1510 and 1460 cm^{-1}) [29]. The spectra of the three samples did not differ significantly from one another. However, the FT-IR spectral intensity of pyrolysis products in the spectrum of EP/2.5% MgAl@NiCo was much lower in the other two samples. The lower intensity of pyrolysis products is attributed to the more compact and cohesive char layer that served as a reinforced barrier, retarding the escape of pyrolysis products. Moreover, the major source of smoke are particles originating from the organic volatile products such as aromatic compounds (Fig. 11b), ether (Fig. 11c) and hydrocarbons (alkane and its derivatives, Fig. 11d). A decrease in these volatiles contributed to suppressing smoke and thereby improved fire safety. In Fig. 11e, both the flame retardant-treated EPs exhibit lower CO emissions than the neat polymer. The CO decrease led to lower smoke toxicity and reduced fire risk. The absorbance intensity for CO_2 of EP/2.5% MgAl@NiCo is similar to that of pristine EP, but higher than that of EP/2.5% MgAl as shown in Fig. 11f, probably because of the high conversion of the partially oxidized product to the fully oxidized one in the presence of NiCo.

3.7. Flame retardant mechanism of LDH hybrid nanomaterial

The mechanism of action of the flame retardant MgAl@NiCo is illustrated in Scheme 3. Although the char residue values for the samples containing 2.5 wt% MgAl and 2.5 wt% MgAl@NiCo were very close after cone calorimeter test, the quality of the char was distinctly different in the two case. The presence of transition metals in MgAl@NiCo could lead to capture of free radicals of the polymer chains during

Table 3
XPS data of the residual chars of EP/2.5% MgAl and EP/2.5% MgAl@NiCo.

		Area			
		EP/2.5% MgAl		EP/2.5% MgAl@NiCo	
Signal	Binding energy (eV)	Exterior char	Interior char	Exterior char	Interior char
C 1s (C—H, C—C)	284.6	41.2	50.8	57.8	64.6
C 1s (C—O)	286.8	54.7	43.4	31.5	28.9
C 1s (C═O)	288.4	3.4	2.6	4.9	2.8
Mg 2p	49.8	3.2	1.7	4.0	1.9
Al 2p	72.9	1.4	0.8	2.0	1.0
Ni 2p	861.3	–	–	2.1	1.1
Co 2p	785.7	–	–	1.5	0.6

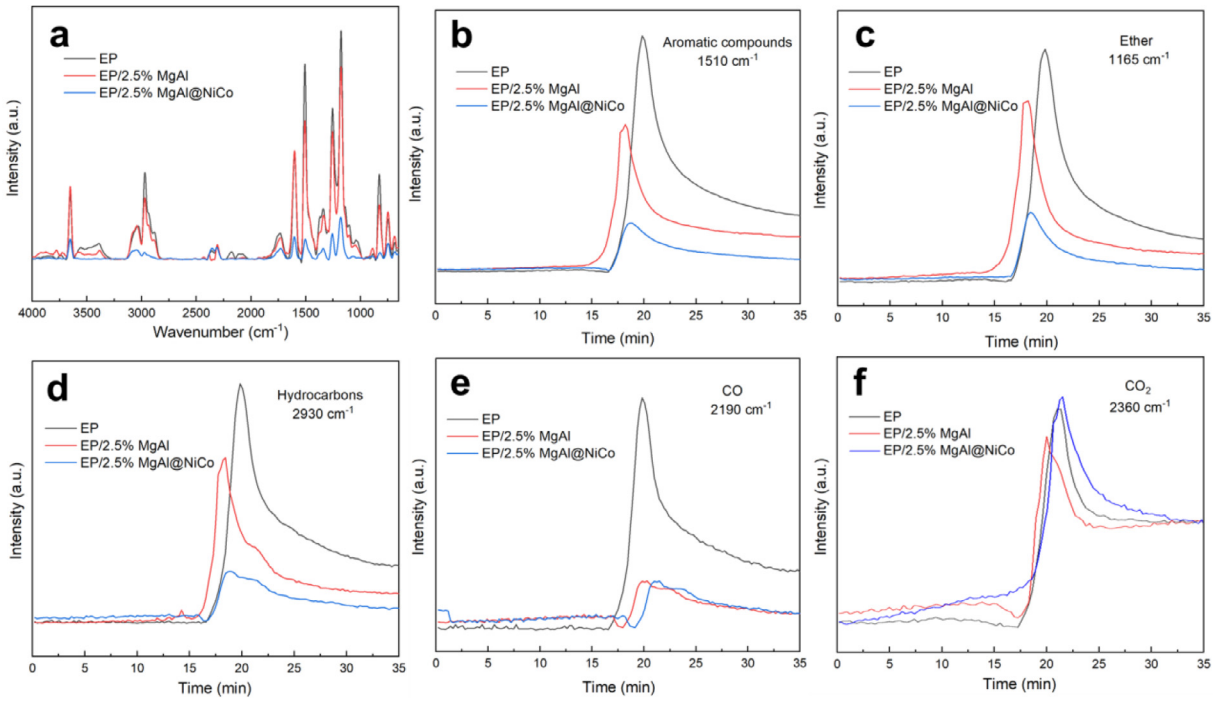

Fig. 11. TG-FTIR results of EP and its nanocomposites: (a) FTIR spectra of pyrolysis products at maximum decomposition rates, (b) aromatic compounds, (c) ether, (d) hydrocarbons, (e) CO and (f) CO_2.

burning and increase the density of crosslinked network. The carbon in the polymer was thus trapped at the front part of combustion, thereby catalytically generating compact char layers to flame retard in the condensed phase, which also led to the reduced smoke production. Even though Ni (II) oxide is colored, no color is detected on the skin layer in Fig. 9c and f, indicating that Ni could be transformed into a higher valence state during burning. Transition metals in MgAl@NiCo were thus able to catalyze the polyaromatic reaction of the pyrolysis products from epoxy to high-quality carbonaceous components, which covered and adhered to the metal oxides formed by the dehydration of MgAl-LDH. The interfacial Ni- and Co-based nano catalysts that were uniformly distributed between MgAl-LDH and the epoxy matrix catalyzed the surrounding areas to form robust char chips, which then combined to form continuous char layers. The resultant carbons with higher mechanical strength and more graphitized ingredients interacted with the degraded volatiles to generate the intumescent char. The incorporation of NiCo-LDH nanosheets also improved the char structure with more effective tiny pore morphology, which reduced less transfer

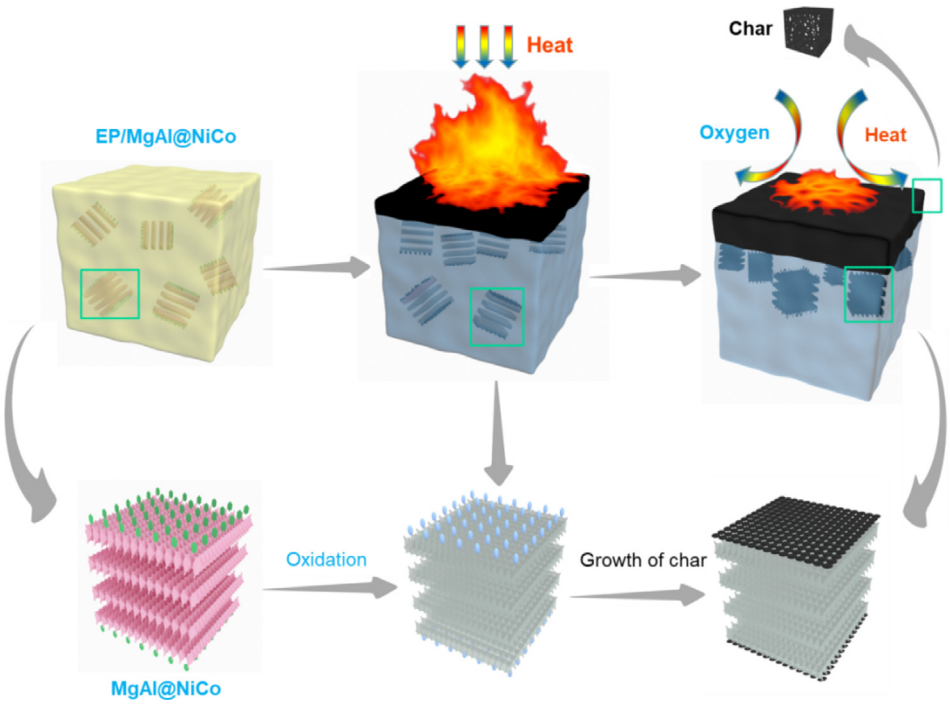

Scheme 3. Flame retardant mechanism for LDHs hybrid nanomaterial in epoxy resin.

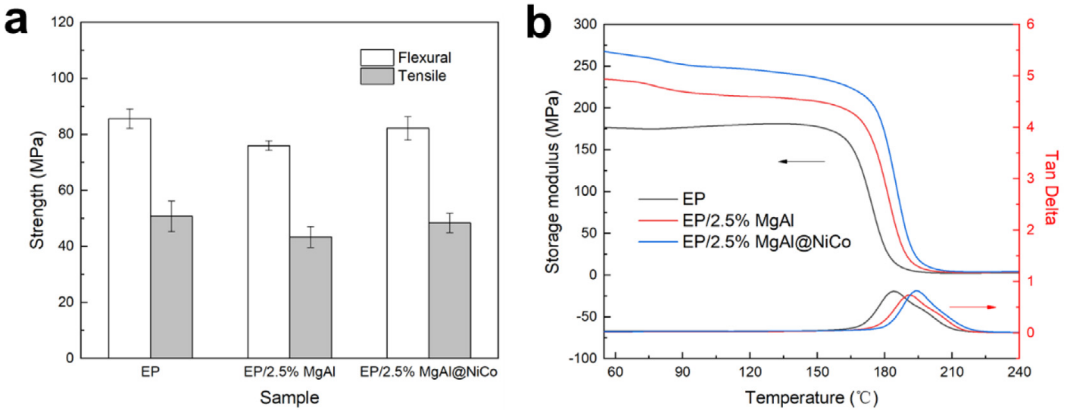

Fig. 12. (a) Flexural and tensile strength, (b) storage modulus and tan delta curves of EP and its nanocomposites.

of heat and flammable volatiles. The synergy between MgAl and NiCo was correlated to the catalytic reaction between MgO and Al_2O_3 formed from MgAl decomposition and NiO and Co_2O_3 that resulted from NiCo decomposition, which added strength to the formed char barrier [30]. The doping of NiCo-LDH nanosheets into the MgAl-LDH thus enabled the formation of stronger char layers and had a synergistic flame-retardant effect.

Apart from the advantageous chemical properties of NiCo-LDH, its superior physical characteristics also contribute to improving the flame retardant efficiency of the as-prepared sample. Owing to the proposed "3D fabrication method", the multiple dimensional nanostructure constituted by NiCo-LDH nanosheets was successfully deposited on the surface of MgAl-LDH platelets and acted as a "spacer" to inhibit the aggloermation of the platelets into large particles, which was beneficial to improving the dispersion of the flame retardant in the epoxy matrix. Moreover, when compared with nanoparticles or flat-lying nanosheets on MgAl-LDH, our designed structure increased the roughness of the MgAl-LDH surface, thereby improving its interfacial interaction with the polymer. All these advantages of MgAl@NiCo boosted flame retardancy of the epoxy nanocomposite.

3.8. Mechanical properties of epoxy nanocomposites

The mechanical properties of epoxy nanocomposites were characterized by using flexural and tensile tests. Fig. 12a presents the flexural and tensile strengths for EP, EP/2.5% MgAl and EP/2.5% MgAl@NiCo. The addition of MgAl@NiCo slightly lowered both flexural and tensile strengths as compared with neat EP, but the values were higher than those of EP/2.5% MgAl. When comparing with MgAl-added nanocomposite, multiple factors may contribute to the better flexural and tensile strengths in MgAl@NiCo-added nanocomposites. One obvious factor is the improved dispersion of the LDHs hybrid nanomaterial in the epoxy matrix (as evidenced in Section 3.2) achieved because of the novel method of nanocasting NiCo-LDH nanosheets on the surface of MgAl-LDH, developed in this study. Another factor might be the improved interfacial interaction between the hybrid filler and the epoxy matrix that facilitated load transfer [31].

Fig. 12b shows the dynamic mechanical properties of EP and its nanocomposites. It can be clearly seen that the addition of MgAl and MgAl@NiCo enhanced storage modulus and glass transition temperature (T_g) of the nanocomposites when tested under shear mode, with MgAl@NiCo showing a better performance. The notable improvement of properties for EP/2.5% MgAl@NiCo was mainly due to the inhibition of motion of the epoxy chain due to the better intercalation of the flame retardant into the matrix, along with finer dispersion nanosheets in the system [32].

4. Conclusions

In this work, NiCo-LDH nanosheets with a multiple dimensional nanostructure derived from MOFs were uniformly modified on the surface of MgAl-LDH through a "3D fabrication method" to prepare a LDH hybrid nanomaterial. The epoxy nanocomposite with only 2.5 wt% MgAl@NiCo passed the UL-94 test with a V-0 rating, while the sample containing the same amount of MgAl showed no rating. The LOI value of the epoxy nanocomposite increased from 23.5 to 26.0% as compared to that of the neat EP. In cone calorimeter tests, the epoxy nanocomposite containing MgAl@NiCo showed lower pHRR, THR, and TSP values in contrast to those of unmodified MgAl-LDH. The enhanced flame-retardant efficiency of MgAl@NiCo was achieved by engineering NiCo-LDH nanosheets on the MgAl-LDH laminates. The advantages of NiCo-LDH for the flame retardant included improved oxidation stability and strength of the char, synergistic flame-retardant effect, and a fine dispersion that allowed stronger interaction within the polymer matrix. The exfoliated dispersion state and rough surface of the nanofiller also improved the mechanical properties of the nanocomposite. The addition of MgAl@NiCo had little effect on flexural and tensile strengths but improved the storage modulus and glass transition temperature of the epoxy nanocomposites. The dual LDH hybrid nanomaterial fabricated successfully for the first time in this study, may play a vital role in fire-safety improvement and in many other areas due to its multiple functions.

Acknowledgments

This research is funded by Beijing Institute of Technology Research Fund Program for Young Scholars (Grant Number: 2019CX04083) and the China Postdoctoral Science Foundation (Grant Number: 2018 M641214).

References

[1] Y.-T. Pan, L. Zhang, X. Zhao, D.-Y. Wang, Interfacial engineering of renewable metal organic framework derived honeycomb-like nanoporous aluminum hydroxide with tunable porosity, Chem. Sci. 8 (2017) 3399–3409.
[2] S.-D. Jiang, G. Tang, J. Chen, Z.-Q. Huang, Y. Hu, Biobased polyelectrolyte multilayer-coated hollow mesoporous silica as a green flame retardant for epoxy resin, J. Hazard. Mater. 342 (2018) 689–697.
[3] B. Yu, Y. Shi, B. Yuan, S. Qiu, W. Xing, W. Hu, L. Song, S. Lo, Y. Hu, Enhanced thermal and flame retardant properties of flame-retardant-wrapped graphene/epoxy resin nanocomposites, J. Mater. Chem. A 3 (2015) 8034–8044.
[4] S. Qiu, Y. Zhou, X. Zhou, T. Zhang, C. Wang, R.K. Yuen, W. Hu, Y. Hu, Air-stable polyphosphazene-functionalized few-layer black phosphorene for flame retardancy of epoxy resins, Small 15 (2019) 1805175.
[5] E.N. Kalali, X. Wang, D.-Y. Wang, Functionalized layered double hydroxide-based epoxy nanocomposites with improved flame retardancy and mechanical properties, J. Mater. Chem. A 3 (2015) 6819–6826.
[6] C. Li, J. Wan, E.N. Kalali, H. Fan, D.-Y. Wang, Synthesis and characterization of functional eugenol derivative based layered double hydroxide and its use as a

nanoflame-retardant in epoxy resin, J. Mater. Chem. A 3 (2015) 3471–3479.
[7] S. Elbasuney, Surface engineering of layered double hydroxide (LDH) nanoparticles for polymer flame retardancy, Powder Technol. 277 (2015) 63–73.
[8] S. Elbasuney, Continuous hydrothermal synthesis of AlO(OH) nanorods as a clean flame retardant agent, Particuology 22 (2015) 66–71.
[9] S. Elbasuney, S.F. Mostafa, Continuous flow formulation and functionalization of magnesium di-hydroxide nanorods as a clean nano-fire extinguisher, Powder Technol. 278 (2015) 72–83.
[10] C.M. Becker, A.D. Gabbardo, F. Wypych, S.C. Amico, Mechanical and flame-retardant properties of epoxy/Mg–Al LDH composites, Composites Part A 42 (2011) 196–202.
[11] S. Elbasuney, H.E. Mostafa, Synthesis and surface modification of nanophosphorous-based flame retardant agent by continuous flow hydrothermal synthesis, Particuology 22 (2015) 82–88.
[12] S. Elbasuney, Sustainable steric stabilization of colloidal titania nanoparticles, Appl. Surf. Sci. 409 (2017) 438–447.
[13] X. Yang, J. Zhu, L. Qiu, D. Li, Bioinspired effective prevention of restacking in multilayered graphene films: towards the next generation of high-performance supercapacitors, Adv. Mater. 23 (2011) 2833–2838.
[14] P.p. Wang, H. Sun, Y. Ji, W. Li, X. Wang, Three-dimensional assembly of single--layered MoS_2, Adv. Mater. 26 (2014) 964–969.
[15] S. Chen, Y. Huang, X. Han, Z. Wu, C. Lai, J. Wang, Q. Deng, Z. Zeng, S. Deng, Simultaneous and efficient removal of Cr (VI) and methyl orange on LDHs decorated porous carbons, Chem. Eng. J. 352 (2018) 306–315.
[16] E.N. Kalali, X. Wang, D.-Y. Wang, Synthesis of a Fe_3O_4 nanosphere@Mg–Al layered-double-hydroxide hybrid and application in the fabrication of multifunctional epoxy nanocomposites, Ind. Eng. Chem. Res. 55 (2016) 6634–6642.
[17] Z. Li, J. Zhang, F. Dufosse, D.-Y. Wang, Ultrafine nickel nanocatalyst-engineering of an organic layered double hydroxide towards a super-efficient fire-safe epoxy resin via interfacial catalysis, J. Mater. Chem. A 6 (2018) 8488–8498.
[18] E. Kandare, A.A. Khatibi, S. Yoo, R. Wang, J. Ma, P. Olivier, N. Gleizes, C.H. Wang, Improving the through-thickness thermal and electrical conductivity of carbon fibre/epoxy laminates by exploiting synergy between graphene and silver nano-inclusions, Composites Part A 69 (2015) 72–82.
[19] J. Xu, S. Gai, F. He, N. Niu, P. Gao, Y. Chen, P. Yang, A sandwich-type three-dimensional layered double hydroxide nanosheet array/graphene composite: fabrication and high supercapacitor performance, J. Mater. Chem. A 2 (2014) 1022–1031.
[20] J. Hu, C. Zhang, L. Jiang, H. Lin, Y. An, D. Zhou, M.K. Leung, S. Yang, Nanohybridization of MoS_2 with layered double hydroxides efficiently synergizes the hydrogen evolution in alkaline media, Joule 1 (2017) 383–393.
[21] L. Yu, Y.-H. Lee, X. Ling, E.J. Santos, Y.C. Shin, Y. Lin, M. Dubey, E. Kaxiras, J. Kong, H. Wang, Graphene/MoS_2 hybrid technology for large-scale two-dimensional electronics, Nano Lett. 14 (2014) 3055–3063.
[22] Y. Liu, N. Wang, J.H. Pan, F. Steinbach, J.R. Caro, In situ synthesis of MOF membranes on ZnAl-CO_3 LDH buffer layer-modified substrates, J. Am. Chem. Soc. 136 (2014) 14353–14356.
[23] Z. Li, M. Shao, L. Zhou, R. Zhang, C. Zhang, M. Wei, D.G. Evans, X. Duan, Directed growth of metal-organic frameworks and their derived carbon-based network for efficient electrocatalytic oxygen reduction, Adv. Mater. 28 (2016) 2337–2344.
[24] X. Wang, E.N. Kalali, D.-Y. Wang, Renewable cardanol-based surfactant modified layered double hydroxide as a flame retardant for epoxy resin, ACS Sustain. Chem. Eng. 3 (2015) 3281–3290.
[25] K. Zhou, J. Liu, Y. Shi, S. Jiang, D. Wang, Y. Hu, Z. Gui, MoS_2 nanolayers grown on carbon nanotubes: an advanced reinforcement for epoxy composites, ACS Appl. Mater. Interfaces 7 (2015) 6070–6081.
[26] Y.-T. Pan, D.-Y. Wang, Fabrication of low-fire-hazard flexible poly (vinyl chloride) via reutilization of heavy metal biosorbents, J. Hazard. Mater. 339 (2017) 143–153.
[27] L. Zhang, Z. Li, Y.-T. Pan, A.P. Yáñez, S. Hu, X.-Q. Zhang, R. Wang, D.-Y. Wang, Polydopamine induced natural fiber surface functionalization: a way towards flame retardancy of flax/poly (lactic acid) biocomposites, Composites Part B 154 (2018) 56–63.
[28] X. Wang, S. Zhou, W. Xing, B. Yu, X. Feng, L. Song, Y. Hu, Self-assembly of Ni–Fe layered double hydroxide/graphene hybrids for reducing fire hazard in epoxy composites, J. Mater. Chem. A 1 (2013) 4383–4390.
[29] S. Qiu, X. Wang, B. Yu, X. Feng, X. Mu, R.K. Yuen, Y. Hu, Flame-retardant-wrapped polyphosphazene nanotubes: a novel strategy for enhancing the flame retardancy and smoke toxicity suppression of epoxy resins, J. Hazard. Mater. 325 (2017) 327–339.
[30] S. Elbasuney, Novel multi-component flame retardant system based on nanoscopic aluminium-trihydroxide (ATH), Powder Technol. 305 (2017) 538–545.
[31] Y.-T. Pan, C. Trempont, D.-Y. Wang, Hierarchical nanoporous silica doped with tin as novel multifunctional hybrid material to flexible poly (vinyl chloride) with greatly improved flame retardancy and mechanical properties, Chem. Eng. J. 295 (2016) 451–460.
[32] H. Yao, S.A. Hawkins, H.-J. Sue, Preparation of epoxy nanocomposites containing well-dispersed graphene nanosheets, Compos. Sci. Technol. 146 (2017) 161–168.